processes

MDPI

Article

Optimal Configuration Method of Energy Routers in Active Distribution Network Considering Demand Response

Junqing Jia [1], Tianyu Wu [2], Jia Zhou [3], Wenchao Cai [1,4], Zehua Wang [4,*], Junda Lu [4], Chen Shao [4] and Jiaoxin Jia [4]

[1] Inner Mongolia Electric Power Research Institute Branch, Inner Mongolia Electric Power (Group) Co., Ltd., Hohhot 010020, China
[2] Inner Mongolia Ultra-High Voltage Power Supply Branch, Inner Mongolia Electric Power (Group) Co., Ltd., Hohhot 010020, China
[3] Aviation Inspection Branch, Inner Mongolia Electric Power (Group) Co., Ltd., Hohhot 010020, China
[4] Hebei Provincial Key Laboratory of Distributed Energy Storage and Microgrid, North China Electric Power University, Baoding 071003, China
* Correspondence: zehua789oo@163.com

Abstract: The energy router (ER) is a crucial component in smart distribution networks, and its optimal configuration is essential for enhancing the operational efficiency, economy, and security of the grid. However, existing research rarely considers both the location and sizing costs of the ER in conjunction with flexible load demand response. Therefore, this paper proposes an optimal configuration method for the energy router in active distribution networks, incorporating demand response. First, to balance the comprehensive operational characteristics of the active distribution network throughout the year with computational efficiency, an improved K-means clustering algorithm is employed to construct multiple representative scenarios. Then, a bi-level programming model is established for ER location and sizing, considering demand response. The upper level optimizes the location and capacity configuration of the ER to minimize the overall cost of the distribution network. The lower level focuses on multi-objective optimization, including peak shaving, valley filling, network losses, and voltage deviations, to achieve energy scheduling within the distribution network. Finally, an improved bi-level particle swarm optimization algorithm is employed to solve the model. Simulation results based on the IEEE 33-node system demonstrate that the peak shaving and valley filling optimization rate after ER integration into the active distribution network is at least 9.19%, and it is improved to 14.35% when combined with demand response. Concurrently, the integration of the ER enhances the distribution network's ability to absorb renewable energy, reduces network losses, and improves power quality.

Keywords: energy router; demand response; bi-level programming model; peak shaving and valley filling; improved bi-level particle swarm optimization

check for updates

Academic Editor: Massimo Caruso

Received: 16 March 2025
Revised: 9 April 2025
Accepted: 14 April 2025
Published: 20 April 2025

Citation: Jia, J.; Wu, T.; Zhou, J.; Cai, W.; Wang, Z.; Lu, J.; Shao, C.; Jia, J. Optimal Configuration Method of Energy Routers in Active Distribution Network Considering Demand Response. *Processes* **2025**, *13*, 1248. https://doi.org/10.3390/pr13041248

Copyright: © 2025 by the authors. Licensee MDPI, Basel, Switzerland. This article is an open access article distributed under the terms and conditions of the Creative Commons Attribution (CC BY) license (https://creativecommons.org/licenses/by/4.0/).

1. Introduction

Driven by the evolution of power systems towards smart, sustainable, and decentralized architectures, active distribution networks (ADNs) are becoming crucial hubs for source–grid–load–storage coordination, and are facing increasingly complex scheduling and management challenges. The integration of large-scale, distributed renewable energy sources (RESs), characterized by intermittency and volatility, introduces significant operational uncertainties, including voltage deviations and increased network losses [1–4]. Therefore, optimizing energy flow, minimizing operational costs, and enhancing system

stability and flexibility are critical research priorities [5–7]. Energy routers (ERs), with their multi-energy flow access and flexible power regulation capabilities, are emerging as key enablers of intelligent evolution in ADNs. ERs provide standardized interfaces for distribution areas, supporting plug-and-play integration of AC/DC equipment such as distributed generation and electric vehicles [8], offering significant advantages in voltage support, power flow control, and cost reduction [9–11]. With the backdrop of the "dual carbon" strategy and the rapid development of integrated energy systems, ER technology is being deployed domestically and internationally. The International Energy Agency (IEA) and other authoritative organizations recognize the critical role of ERs in multi-energy flow coordination and regional energy autonomy. However, the investment cost of ERs necessitates careful consideration of their optimal siting and capacity planning.

Recent research has extensively explored ER configuration optimization. Reference [12] proposed an optimized configuration strategy for multi-port energy routers, focusing on storage capacity optimization to minimize overall costs. References [13,14] optimized ER capacity and regional energy network planning based on routing algorithms and inter-regional power interaction, respectively, enhancing the economic efficiency and reliability of the system. Reference [15] utilized a multi-agent coordination mechanism for the integrated planning of ER clusters and the distribution network, optimizing internal equipment capacity and adjusting the distribution network structure to improve RES integration and line utilization. Furthermore, Reference [16] investigated the joint optimization of distributed photovoltaics and hybrid energy storage to enhance renewable energy absorption and system flexibility. Reference [17] proposed an ER cluster optimal siting method, incorporating a voltage sensitivity-based evaluation index to improve distribution network voltage profiles, providing balanced siting references for multi-source load access. References [18–20] considered the fluctuations and uncertainties in wind power, solar radiation, and electricity demand, proposing planning methods for distributed generation and ERs based on scenario modeling and optimization algorithms, with the objective of minimizing overall costs. Reference [21] presented a collaborative optimization strategy for integrated energy systems and distribution networks based on ERs, employing an improved particle swarm optimization method to enhance supply reliability, reduce carbon emissions, and construct a stable, low-carbon integrated energy system.

Although existing studies have made progress in ER capacity configuration, significant challenges remain in practical engineering applications. First, most research focuses on capacity configuration while neglecting the siting problem. This can lead to ER placement that is uncoordinated with the distribution network structure, resulting in voltage deviations, increased line losses, and, consequently, reduced system operational efficiency and stability [22,23], as observed in the early phases of projects like the Rudong wind power grid connection project in Jiangsu, China, the Jining integrated energy pilot in Shandong, China, and the Low Carbon London project in the UK. Second, flexible load demand response (FLDR), an important mechanism for enhancing system dynamic regulation, has been widely applied for load shaping and peak shaving [24,25]. However, few existing studies systematically incorporate FLDR into ER siting and sizing optimization models, hindering the ability to simultaneously address resource allocation and operational regulation. Furthermore, current approaches often rely on traditional intelligent algorithms such as particle swarm optimization and genetic algorithms, or commercial solvers, which can become trapped in local optima when handling large-scale, multi-constrained, nonlinear mixed-integer problems. This results in high computational complexity, low solving efficiency, and limited engineering applicability.

To address these challenges, this study proposes an ER siting and sizing method that integrates FLDR and an improved two-layer particle swarm optimization algorithm, aiming

to simultaneously optimize ER location, capacity configuration, and flexible load scheduling within the distribution network. The main contributions are as follows: (1) a joint optimization method for ER siting and capacity configuration, incorporating FLDR mechanisms to enhance system flexibility and coordination, is proposed; (2) an improved K-means clustering method is introduced to construct typical operating scenarios, with the Calinski–Harabasz index, enhancing clustering effectiveness; (3) a two-layer ER configuration-scheduling model is developed, with the upper layer minimizing investment and operating costs, and the lower layer considering network loss, voltage deviation, and peak shaving; (4) an improved two-layer particle swarm algorithm integrating multiple strategies is designed to enhance search capability and convergence performance; (5) the proposed model is validated using the IEEE 33-node system, evaluating its advantages in terms of economic efficiency, scheduling performance, and engineering applicability; and (6) a sensitivity analysis of the flexible load participation ratio is performed to systematically assess the impact of key parameter variations on siting, sizing, and operational performance, further verifying the model's adaptability and engineering robustness under different operating conditions.

2. Modeling of Multiple Scenarios Considering Uncertainty in Generation and Load

In the planning and operation of active distribution networks, wind power, photovoltaic generation, and load are significantly influenced by factors such as weather and time, exhibiting considerable volatility and uncertainty. This results in continuously changing operational conditions, which directly impact the optimization of energy router configurations. If different operational scenarios are not considered, the dual-level planning scheme for site selection and capacity sizing may struggle to adapt to complex conditions in actual operation, thus reducing both the system's safety and economic performance.

To ensure that the optimization of energy router configurations can accommodate the dynamic characteristics of renewable energy generation and load demand, it is necessary to establish multiple operational scenarios. A single scenario is insufficient to comprehensively capture the system's operational characteristics, and relying solely on data from specific moments for optimization may lead to a lack of adaptability in the site selection and capacity sizing schemes during actual operations. Therefore, to accurately describe the temporal variation of renewable energy generation and load characteristics while balancing optimization accuracy and efficiency, a multi-scenario modeling approach is adopted. This method substitutes the complete set of all possible scenarios with a limited number of typical scenarios, improving computational efficiency while ensuring the representativeness of the selected scenarios.

Specifically, the operational scenarios are first constructed based on wind power, photovoltaic generation, and load data. Key statistical features are extracted to describe the changing trends under different time series, as shown in Equation (1):

$$\begin{cases} d_1 = \dfrac{1}{T}\sum\limits_{t=1}^{T} P_{i,t} \\ d_2 = \dfrac{1}{T}\sum\limits_{t=1}^{T} (P_{i,t} - d_1)^2 \\ d_3 = \max(P_{i,t}), t \in [1, 24] \\ d_4 = \max(P_{i,t}) - \min(P_{i,t}), t \in [1, 24] \\ d_5 = \dfrac{1}{T}\sum\limits_{t=1}^{T} \dfrac{d_1}{d_3} \end{cases} \tag{1}$$

In the equation, d_1 represents the average daily output of the i energy source; $P_{i,t}$ refers to wind power, photovoltaic, and load; $P_{i,t}$ is the output at time t; T represents the 24 h in a day; d_2 is the variance of the daily output of the i source; d_3 is the peak daily output of the i source; d_4 is the peak-valley difference of the i source's daily output; d_5 is the daily load rate.

Next, unlike dimensionality reduction methods such as PCA, K-means preserves the spatial distribution and physical meaning of time series data like load output without disrupting the original data structure; therefore, the K-means algorithm is chosen for typical scenario clustering. However, the K-means algorithm requires pre-setting the number of clusters, and subjective determination may lead to unstable clustering results, which affects the accuracy of energy router site selection and capacity sizing, thereby reducing the reliability and precision of the system optimization. To improve the objectivity and representativeness of the clustering analysis, the Calinski–Harabasz (CH) index is introduced to improve the K-means algorithm by automatically determining the optimal number of clusters, thereby enhancing the rationality of scenario partitioning. A higher CH index indicates better clustering. For specific steps of the K-means algorithm, refer to [26].

The calculation formula for the CH index is given by Equation (2).

$$\begin{aligned} CH &= \frac{SS_{\mathrm{B}}/(k-1)}{SS_{\mathrm{W}}/(N-k)} \\ SS_{\mathrm{B}} &= \sum_{i=1}^{k} n_i \|c_i - c\|^2 \\ SS_{\mathrm{W}} &= \sum_{i=1}^{k} \sum_{x \in C_i} \|x - c_i\|^2 \end{aligned} \tag{2}$$

In the equation, SS_{B} represents the sum of squares between clusters; SS_{W} denotes the sum of squares within clusters; N is the total number of samples; k is the number of clusters; n_i is the number of samples in the i cluster; c_i is the centroid of the i cluster; c is the global centroid of all samples; C_i represents the i cluster; and x is a sample in the i cluster.

3. Energy Router Location and Sizing Bi-Level Planning Model

3.1. Planning Framework

To appropriately handle model coupling issues stemming from the inconsistencies in objectives and variations in temporal scales between planning and operation levels, this paper proposes a bi-level configuration model for the joint optimization of energy router planning and operation across multiple scenarios, as shown in Figure 1. Initially, supervised clustering is applied to the annual data of wind and solar power generation and load consumption to extract typical scenarios, which are then fed into the bi-level planning model.

In the planning level, the objective is to minimize the comprehensive cost of the active distribution network, which includes both investment and construction costs as well as the operational economic costs derived from the feedback from the operation level. The model optimizes the location and capacity configuration of energy routers and passes the solution to the operation level.

At the operation level, based on the configuration determined in the planning level, the operation strategy of the distribution network is optimized, with a focus on ensuring system security, including node voltage deviation, network losses, and load peak–valley differences. The operation level optimizes the distribution network's operation under various typical scenarios and calculates the operational economic cost for each scenario. Finally, the weighted operational cost is obtained by combining the occurrence probability of each scenario, which is then fed back to the planning level.

Ultimately, the planning level selects the optimal energy router configuration based on the integrated optimization of investment construction costs and operational economic costs, ensuring both the economy and security of the active distribution network.

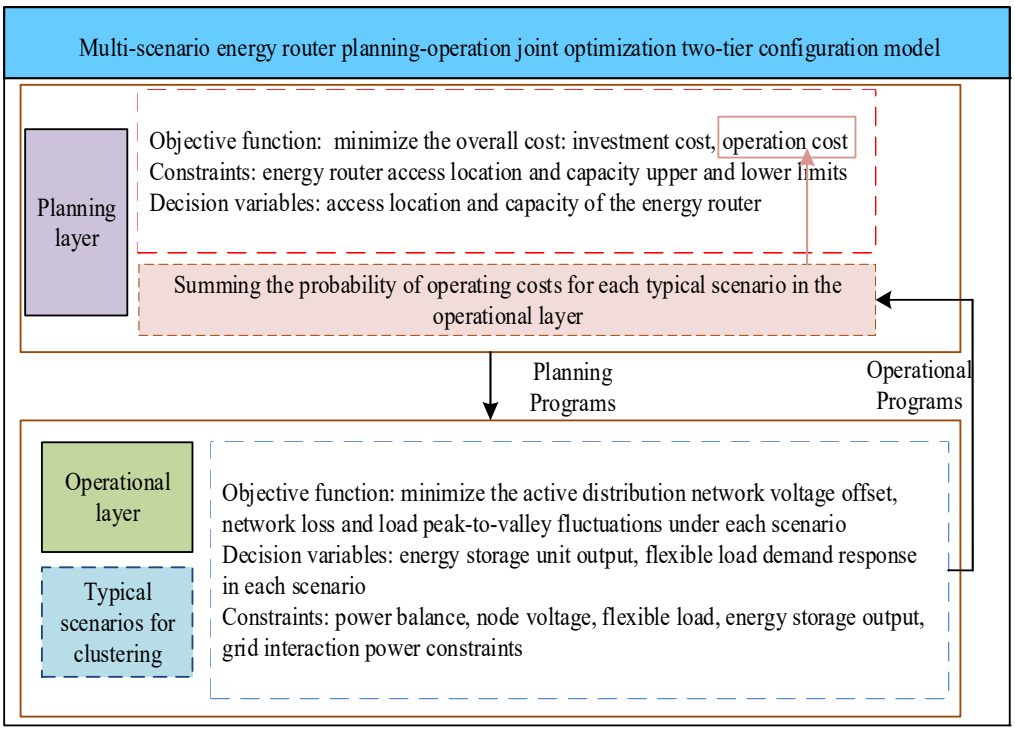


Figure 1. Double-layer model optimization frame diagram.

3.2. Planning Layer Model

3.2.1. Objective Function

The upper-level planning aims to minimize the comprehensive cost of integrating the energy router (ER) into the distribution network. This includes both the investment construction cost and the operational economic cost from the lower-level feedback. The objective function is shown in Equation (3).

$$\min(C_{\text{plan}}) = C_{\text{inv}} + C_{\text{low}} \tag{3}$$

In the equation, C_{plan} is the comprehensive cost of the planning layer, including the investment construction cost C_{inv} and the operating economic cost C_{low} of the lower feedback.

The ER's investment construction cost is matched with the operation optimization period and converted into daily investment costs.

$$C_{\text{inv}} = \frac{1}{365}\left(\frac{r \cdot (1+r)^n}{(1+r)^n - 1}\right) \cdot C_1 \cdot P_{\text{g}} \tag{4}$$

In the equation, C_{inv} represents the ER's investment construction cost; C_1 represents the unit capacity cost of the ER; P_{g} active_capacity represents the active capacity connected by the ER; r represents the discount rate; and n represents the investment recovery period in years.

The operational economic cost from the lower-level feedback includes the transaction cost between the active distribution network and the external grid, equipment maintenance cost, and the incentive cost for flexible load response, as shown in Equation (5).

$$\begin{aligned} C_{\text{low}} &= \sum_{i=1}^{N} p_i \cdot C_{\text{pri_}i} \\ C_{\text{pri_}i} &= C_{\text{yw_}i} + C_{\text{inc_}i} \\ C_{\text{yw_}i} &= C_{\text{yx_}i} + C_{\text{wh_}i} \\ C_{\text{yx_}i} &= \gamma_{\text{gd}} \sum_{t=1}^{T} P_{\text{gen},t} \\ C_{\text{wh_}i} &= \gamma_{\text{whf}} \sum_{t=1}^{T} P_{\text{fj},t} + \gamma_{\text{whg}} \sum_{t=1}^{T} P_{\text{gf},t} + \gamma_{\text{whc}} \sum_{t=1}^{T} P_{\text{cn},t} \\ C_{\text{inc_}i} &= \sum_{t=1}^{T} \left(p_{\text{a_}t}(P_{\text{load_}t} + P_{\text{SL_}t} + P_{\text{CL_}t}) - p_{\text{b_}t} P_{\text{load_}t}\right) + C_{\text{b}} \end{aligned} \tag{5}$$

In the equation, N represents the number of scenarios; p_i represents the probability of the i scenario; $C_{\text{pri_}i}$ represents the operational economic cost of the i scenario; $C_{\text{yx_}i}$ represents the operational and maintenance cost of the $C_{\text{wh_}i}$ scenario, which includes transaction costs with the external grid and equipment maintenance costs; $C_{\text{inc_}i}$ represents the flexible load response incentive cost for the i scenario; γ_{gd} represents the unit electricity purchase price; $P_{\text{gen},t}$ represents the input power from the external grid; γ_{whf} represents the unit capacity maintenance cost of wind turbines; γ_{whg} represents the unit capacity maintenance cost of photovoltaics; γ_{whc} represents the unit capacity maintenance cost of ERs; $P_{\text{fj},t}$ represents the wind turbine power generation; $P_{\text{gf},t}$ represents the photovoltaic power generation; $P_{\text{cn},t}$ represents the energy storage output of the ER; $p_{\text{a_}t}$ represents the time-of-use electricity price; $p_{\text{b_}t}$ represents the traditional electricity price; $P_{\text{SL_}t}$ represents the shiftable load power; $P_{\text{CL_}t}$ represents the curtailable load power; $P_{\text{load_}t}$ represents the original load; and C_{b} represents the compensation constant.

3.2.2. Constraints

The upper-level optimization determines the access location and capacity configuration of the energy routers in the active distribution network, subject to the constraints shown in Equation (6).

$$\begin{aligned} &1 < L_{\text{ER}} \le L_{\text{N}} \\ &S_{\text{ER}_{\text{min}}} \le S_{\text{ER}} \le S_{\text{ER}_{\text{max}}} \end{aligned} \tag{6}$$

In the equation, L_{ER} represents the access location of the energy router; L_{N} represents the number of active distribution network nodes; $S_{\text{ER}_{\text{min}}}$ represents the minimum capacity of the energy router; S_{ER} represents the access capacity of the energy router; and $S_{\text{ER}_{\text{max}}}$ represents the minimum capacity of the energy router.

3.3. Operation Layer Model

3.3.1. Objective Function

To ensure the safe and stable operation of the active distribution network, the lower-level operation aims to optimize the system's operational security. This includes voltage deviation, network loss, and the peak–valley fluctuation of the load curve, as shown in Equation (7).

$$\min F = [V_{\text{dy}}, P_{\text{fg}}, P_{\text{loss}}] \tag{7}$$

Node voltage is a key indicator of the stability of the distribution network and the quality of electric power. Network loss and the peak–valley fluctuations of the load curve affect the system's operational efficiency and reliability, as shown in Equation (8).

$$\begin{cases} V_{\mathrm{dy}} = \sum_{i=1}^{L_{\mathrm{N}}} \sum_{t=1}^{T} \left| V_{it} - \overline{V}_i \right| \\ P_{\mathrm{fg}} = P_{\max} - P_{\min} \\ P_{\mathrm{loss}} = \sum_{k=1}^{l} \left(P_{\mathrm{start}} - P_{\mathrm{end}} \right) \end{cases} \tag{8}$$

In the equation, V_{dy} represents the voltage deviation of the distribution network; L_{N} represents the number of active distribution network nodes; V_{ij} represents the voltage at node i at time t; $\overline{V}_i$ represents the average voltage at node i for the day; P_{fg} represents the peak-valley fluctuation of the load curve; $P_{\max}$ represents the peak value of the load curve; $P_{\min}$ represents the valley value of the load curve; P_{loss} represents the active power loss in the distribution network; l represents the number of branches; P_{start} represents the incoming active power at the starting node; and P_{end} represents the outgoing active power at the ending node.

3.3.2. Constraints

1. Power Balance Constraint

The power balance constraint is expressed as follows:

$$P_{\mathrm{gen},t} + P_{\mathrm{fj},t} + P_{\mathrm{gf},t} + P_{\mathrm{cn},t} = P_{\mathrm{load_}t} + P_{\mathrm{SL_}t} + P_{\mathrm{CL_}t} \tag{9}$$

In the equation, $P_{\mathrm{gen},t}$ represents the input power from the external grid; $P_{\mathrm{fj},t}$ represents the wind turbine power generation; $P_{\mathrm{gf},t}$ represents the photovoltaic power generation; $P_{\mathrm{cn},t}$ represents the energy storage output of the energy router; $P_{\mathrm{load_}t}$ represents the original load power; $P_{\mathrm{SL_}t}$ represents the shiftable load power; and $P_{\mathrm{CL_}t}$ represents the curtailable load power.

2. Node Voltage Constraint

To ensure the safe operation of the distribution network, the voltage at each node must remain within the allowable range, as specified by the following constraint:

$$V_{\min} \le V_i \le V_{\max} \; i = 1, 2, \cdots, n \tag{10}$$

In the equation, $V_{\min}$ and $V_{\max}$ represent the lower and upper limits of the node voltage, respectively; V_i represents the voltage magnitude at node i; and n represents the number of nodes in the network.

3. Flexible Load Constraints

a. shiftable Load Constraint

Shiftable loads can be scheduled at different time periods, but their total power demand remains unchanged. For detailed modeling, please refer to references [27,28]. The constraint is expressed as follows:

$$\begin{aligned} & \alpha_{\mathrm{SL}} P_{\mathrm{SL_min}} \le P_{\mathrm{SL_}t} \le \alpha_{\mathrm{SL}} P_{\mathrm{SL_max}} \\ & P_{\mathrm{SL}'} = P_{\mathrm{SL0}} + P_{\mathrm{SL_}t} \\ & \sum_{t=1}^{T} P_{\mathrm{SL_}t} \Delta t = 0 \\ & \sum_{t=1}^{T} \alpha_{\mathrm{SL}} \le N_{\mathrm{SL,max}} \end{aligned} \tag{11}$$

In the equation, P_{SL_t} represents the shiftable load power; P_{SL_min} and P_{SL_max} represent the minimum and maximum shiftable load power, respectively; α_{SL} is a binary variable indicating whether the shiftable load participates in response; P_{SL0} and $P_{SL'}$ represent the power before and after the transfer of the shiftable load, respectively; and $N_{SL,max}$ represents the maximum number of responses for the shiftable load.

b. Curtailable Load Constraint

Curtailable loads are loads that can be reduced within a certain range without affecting the overall system operation or the core load demand of the user. These loads cannot be completely transferred. For detailed modeling, please refer to references [27,28]. The constraint is expressed as follows:

$$\begin{aligned} &P_{CL_t} = \alpha_{CL}\beta_{CL}P_{CL0} \\ &P_{CL'} = P_{CL0} + P_{CL_t} \\ &t_{CLmin} \le \alpha_{CL}t \le t_{CLmax}(t = 1, 2, \cdots T) \end{aligned} \tag{12}$$

In the equation, P_{CL_t} represents the curtailable load power; α_{CL} is a binary variable indicating whether the curtailable load participates in response; β_{CL} represents the reduction factor of the curtailable load; P_{CL0} and $P_{CL'}$ represent the power before and after the reduction of the curtailable load, respectively; t_{CLmin} and t_{CLmax} represent the lower and upper limits of the response period.

4. Energy Storage Output Constraint

The energy storage unit of the energy router must satisfy energy conservation and output constraints, as expressed in the following equation:

$$\begin{aligned} &\eta^{cn}(E_t^{cn} - E_{t-1}^{cn}) = -P_{cn,t}\Delta t \\ &|P_{cn,min}| \le |P_{cn,t}| \le |P_{cn,max}| \\ &soc_{min} \le \frac{E_t^{cn}}{E^{cn}} \le soc_{max} \\ &soc_{start} = soc_{end} \\ &\sum_{t=1}^{T} P_{cn,t}\Delta t = 0 \end{aligned} \tag{13}$$

In the equation, E_{t-1}^{cn} and E_t^{cn} represent the storage capacity at time $t-1$ and t, respectively; $P_{cn,t}$ represents the energy storage output, where a positive value indicates discharge and a negative value indicates charge; η^{cn} represents the charge/discharge efficiency of the storage unit; $P_{cn,max}$ and $P_{cn,min}$ represent the upper and lower limits for charging/discharging, respectively; E^{cn} represents the rated capacity of the storage unit; soc_{min} and soc_{max} represent the lower and upper limits of the state of charge (SOC); soc_{start} and soc_{end} represent the SOC at 00:00 and 24:00, respectively.

5. Grid Interaction Constraint

At any given time, the power purchased from the external grid by the distribution network must not exceed the system's maximum load demand to ensure the stability of the grid operation and the balance between supply and demand. This is expressed by the following constraint:

$$P_{gen,min} \le P_{gen,t} \le P_{gen,max} \tag{14}$$

In the equation, $P_{gen,min}$ and $P_{gen,max}$ represent the lower and upper limits of the external grid input power, respectively.

4. Energy Router Bi-Level Planning Model Solution

For the bi-level planning model of the energy router (ER) location and capacity determination, the solution process requires parameter interaction between the upper-level

planning and the lower-level operation optimization. The lower-level optimization is a multi-objective nonlinear problem, involving multiple scenarios, large-scale data, and complex constraints. Traditional methods, such as second-order cone programming, struggle with non-convex constraints and mixed-integer variables. The weighted sum method is influenced by weight setting and normalization, making it difficult to comprehensively obtain Pareto optimal solutions. Therefore, an improved bi-level particle swarm optimization algorithm is proposed to improve solution efficiency and ensure the economic and safe configuration of the energy router.

4.1. Improved Bi-Level Particle Swarm Algorithm

Particle swarm optimization (PSO) simulates the collaboration and evolutionary mechanisms of biological groups, offering strong global optimization ability and convergence efficiency [29]. However, it still has limitations in terms of convergence accuracy and computational efficiency. Therefore, this paper adopts an improved bi-level PSO algorithm. The upper-level optimization uses a single-objective PSO, and the lower-level optimization uses a multi-objective PSO to enhance the optimization scheduling performance of the energy router in the active distribution network.

1. Chaotic Initialization

Traditional PSO algorithms may lead to uneven distribution of initial particles in the solution space, which affects the optimization result. To address this, Bernoulli chaotic initialization is used to enhance the uniform distribution of initial solutions and improve solution accuracy, as shown in Equation (15):

$$x_{k+1} = \begin{cases} x_k/(1-\lambda), & x_k \in (0, 1-\lambda] \\ (x_k - 1 + \lambda)/\lambda, & x_k \in (1-\lambda, 1) \end{cases} \tag{15}$$

In the equation, λ represents the chaotic model mapping parameter, and x_k represents the particle position.

2. Adaptive Inertia Weight

The inertia weight influences the algorithm's performance. A larger weight enhances global search capability, while a smaller weight accelerates convergence. A dynamic inertia weight is adopted to adaptively adjust the search range, balancing global optimization and local search ability, as shown in Equation (16):

$$w = \begin{cases} w_{\max} - \frac{(w_{\max} - w_{\min}) \cdot (f - f_{\min})}{f_{avg} - f_{\min}} & f \le f_{avg} \\ w_{\max} & f > f_{avg} \end{cases} \tag{16}$$

In the equation, f represents the fitness value of the particle, and f_{avg} and $f_{\min}$ represent the average and minimum fitness values of all particles, respectively.

3. Dynamic Learning Factors

To prevent premature convergence of particles in the early stages and to enhance global search ability, a strategy is adopted where the group learning factor decreases monotonically and the individual learning factor increases monotonically. This approach accelerates later-stage convergence to the global optimal solution, as shown in Equation (17):

$$\begin{cases} c_1 = 2\sin^2[\frac{\pi}{2}(1 - \frac{m}{M_{\max}})] \\ c_2 = 2\sin^2(\frac{\pi m}{2M_{\max}}) \end{cases} \tag{17}$$

In the equation, m represents the current iteration number, and $M_{\max}$ represents the maximum number of iterations.

4. Combination of Cauchy Mutation and Reverse Learning Strategy

To avoid particles getting trapped in local optima, a reverse learning strategy is introduced to improve solution diversity. This is combined with the Cauchy mutation strategy to expand the search range, enhancing the optimization performance of the upper-level PSO algorithm [30]. This is expressed in Equation (18):

$$\begin{cases} X'_{best}(m) = ub + r \oplus (lb - X_{best}(m)) \\ b_1 = (M_{\max} - \frac{m}{M_{\max}})^m \\ X_{i,j}^{m+1} = X'_{best}(m) + b_1 \oplus (X_{best}(m) - X'_{best}(m)) \\ \eta = \tan[(\xi - 0.5)\pi] \\ X_{i,j}^{m+1} = X_{best}(m) + \eta \oplus X_{best}(m) \end{cases} \tag{18}$$

In the equation, lb and ub represent the lower and upper bounds of the position, respectively; r is a random variable uniformly distributed in (0, 1); $X'_{best}(m)$ represents the reverse solution of the m optimal solution; b_1 is the information exchange parameter; ξ obeys the standard uniform distribution; η is the generating function of random variables; $X_{i,j}^{m+1}$ is the new position for the $m+1$ time.

To further improve optimization performance, a dynamic selection mechanism combined with a greedy rule is used to update the target position through reverse learning and Cauchy mutation strategies. The dynamic selection mechanism is given by Equation (19):

$$\begin{aligned} P_s &= -\exp(1 - \tfrac{m}{M_{\max}})^{20} + 0.05 \\ X_{best} &= \begin{cases} X_{i,j}^{m+1}, f(X_{i,j}^{m+1}) < f(X_{best}) \\ X_{best}, f(X_{i,j}^{m+1}) \geq f(X_{best}) \end{cases} \end{aligned} \tag{19}$$

In the equation, $f(x)$ represents the particle's fitness.

5. Multi-Objective Decision Based on Entropy-Weighted TOPSIS

For the obtained set of Pareto front solutions, the entropy-weighted TOPSIS method is used to evaluate and select the optimal solution [29].

To eliminate the differences in the units of objectives, data are first standardized. Then, based on the objective attributes, the ideal best and worst solutions are determined. The distances between each solution and the ideal best solution are calculated to select the best solution, as shown in Equation (20):

$$\begin{cases} f'_m(x_i) = \dfrac{f_m(x_i)}{\sqrt{\sum_{i=1}^{N} f_m^2(x_i)}} \quad m = 1, 2, \cdots, n \\ d(x_i) = \dfrac{d_+(x_i)}{d_+(x_i) + d_-(x_i)} \\ d_+(x_i) = \sqrt{\sum_{m=1}^{n} [\lambda_m f'_m(x_i) - \lambda_m f'_{m+}]^2} \\ d_-(x_i) = \sqrt{\sum_{m=1}^{n} [\lambda_m f'_m(x_i) - \lambda_m f'_{m-}]^2} \end{cases} \tag{20}$$

In the equation, $f'_m(x_i)$ represents the value of the x_i solution after standardization; $d_+(x_i)$ and $d_-(x_i)$ represent the distances from the x_i solution to the positive and negative ideal solutions, respectively; λ_m is the weight of the f_m objective; f'_{m+} and f'_{m-} represent the best and worst values of the f_m objective after standardization across all solutions.

4.2. Bi-Level Planning Model Solution Process

The bi-level particle swarm optimization (PSO) algorithm is structured as an upper-lower cooperative optimization framework. The upper level optimizes the location and capacity configuration of the energy routers, while the lower level optimizes the distribution network's operation under typical scenarios. These two levels continuously interact throughout the optimization process, ensuring the economic and safety performance of the final solution. The specific process is shown in Figure 2.

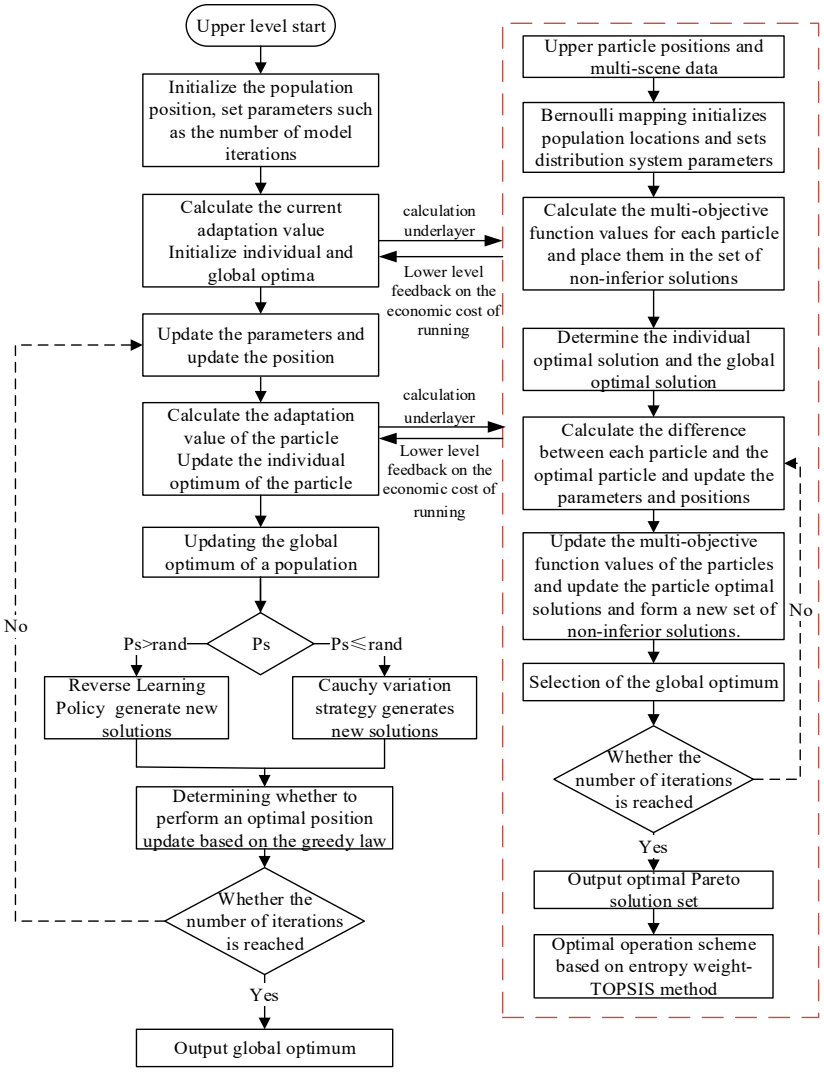


Figure 2. Improved solution process of two-layer particle swarm optimization.

1. Population Initialization

Upper level: Set the population size, inertia weight, learning factors, and other parameters. Initialize the particle positions and velocities, and define the fitness function with investment costs and the operational costs from the lower-level feedback as optimization objectives.

Lower level: Use Bernoulli chaotic initialization to optimize the particle distribution, ensuring uniformity in the initial solution. Set multi-objective functions and configure the parameters of the distribution network system.

2. Fitness Calculation

Upper level: Calculate the current particle's fitness value, record the individual best and global best, and pass the current location and capacity configuration parameters to the lower level.

Lower level: Based on the upper-level solution, calculate the distribution network's operating state, including power flow calculations, node voltages, network losses, and load fluctuations. Then, compute the operational costs under different scenarios and feedback this information to the upper level.

3. Update Particle Position

Update the positions and velocities of the particles based on their fitness values. Use dynamic inertia weights and learning factor strategies to balance global exploration and local convergence, enhancing the optimization stability.

4. Interactive Optimization

Upper level: Use the reverse learning and Cauchy mutation strategies to update particle positions and pass the new positions to the lower level.

Lower level: Re-optimize the operating state based on the new parameters provided by the upper level, update the fitness values, and return the updated operational costs.

5. Select Optimal Solution

Upper level: If the fitness value of the particle swarm stabilizes, convergence is achieved, and the optimal location and capacity configuration plan is output. If not, continue the iteration process.

Lower level: Compute the Pareto front solutions, use the entropy-weighted TOPSIS method to make decisions, select the optimal operational solution, and feedback the final operational cost to the upper-level.

6. Termination Criteria

If the upper-level fitness function value no longer changes after several iterations, the optimal solution is obtained. Output the final energy router configuration and the optimal operational scheduling strategy.

5. Case Study Analysis

5.1. Case Setup

This case study is based on the IEEE 33-bus system. The improved bi-level particle swarm optimization algorithm was implemented using MATLAB scripts (R2023a; MathWorks Inc., Natick, MA, USA), with the CPLEX toolbox for optimization (CPLEX Optimization Studio, version 12.10; IBM Corporation, Armonk, NY, USA). The test system hardware environment was an Intel(R) Core(TM) i7-10750H CPU, with a clock speed of 2.60 GHz, 16.0 GB of RAM, and an operating system of Windows 10 64-bit.

The specific structure of the IEEE 33-bus system is shown in Figure 3. The base voltage is 12.66 kV and the base capacity is 10 MVA. The photovoltaic systems are connected to nodes 9 and 30, while the wind turbines are connected to nodes 14 and 20. The operating records of a distribution system in a real-world region are used, encompassing hourly load consumption, photovoltaic generation, and wind power output data for 365 days. Time-of-use electricity prices are set with peak periods from 09:00 to 12:00 and 19:00 to 22:00, with a price of 1.09 yuan/(kW·h). The off-peak period is from 00:00 to 08:00, with a price of 0.35 yuan/(kW·h), and the remaining hours are considered off-peak with a price of 0.68 yuan/(kW·h). The shiftable load accounts for 30% of the total load, and the curtailable load accounts for 15%.

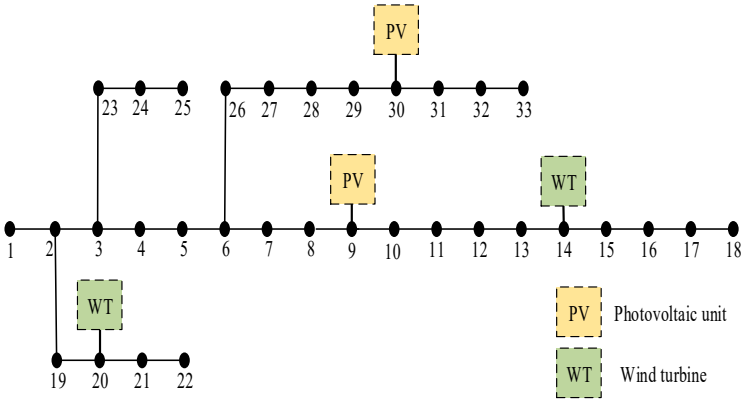


Figure 3. Thirty-three-node active distribution network.

5.2. Plan Setup

To verify the effectiveness of the method proposed in this paper, the following four scenarios are set for comparison:

Scenario 1: No demand response considered, bi-level planning of the energy router in a single scenario.

Scenario 2: Demand response considered, bi-level planning of the energy router in a single scenario.

Scenario 3: No demand response considered, bi-level planning of the energy router in multiple scenarios.

Scenario 4: Demand response considered, bi-level planning of the energy router in multiple scenarios.

5.3. Simulation Results

1. Multi-Scenario Clustering

Clustering was performed on the annual output data of photovoltaic (PV) systems, wind turbines, and daily load consumption. The variation in clustering validity indicators for different numbers of clusters is shown in Figure 4. The clustering validity indicator reaches its maximum value when the number of clusters is 4, so the optimal number of clusters is determined to be 4. The probabilities of the four typical scenarios are shown in Table 1, and the daily output curves of the PV systems, wind turbines, and load for these four typical scenarios are shown in Figures 5–7.

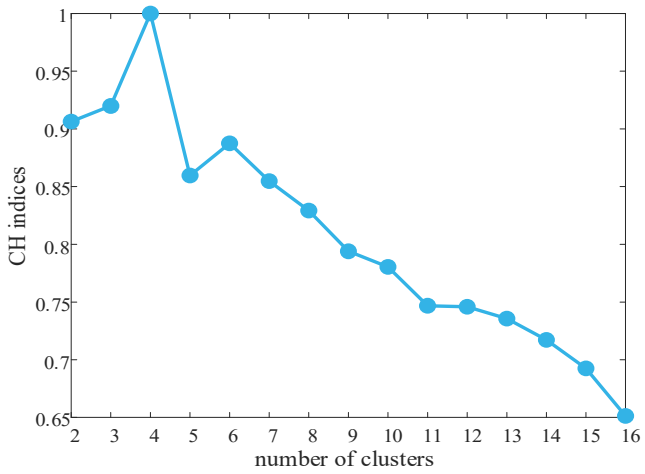


Figure 4. Effectiveness index curve.

Table 1. Typical scenario probability.

Scene Clustering	Scenario Probability
Scene 1	0.083
Scene 2	0.334
Scene 3	0.227
Scene 4	0.356

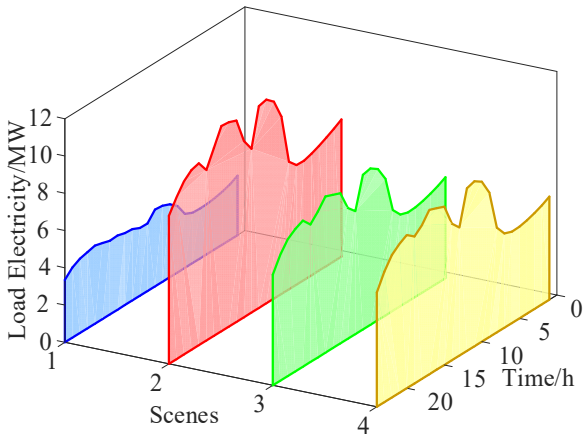


Figure 5. Load active power in typical scenarios.

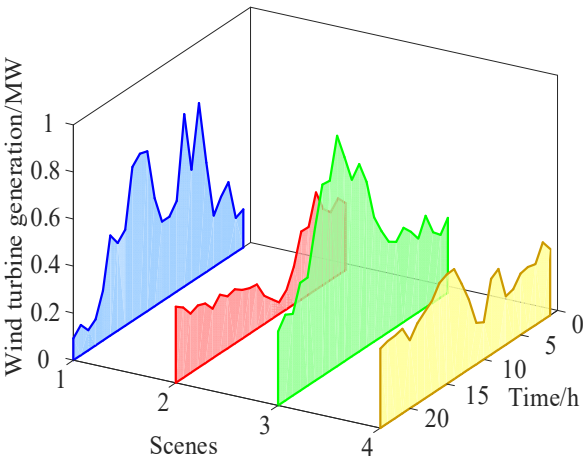


Figure 6. Wind power in typical scenarios.

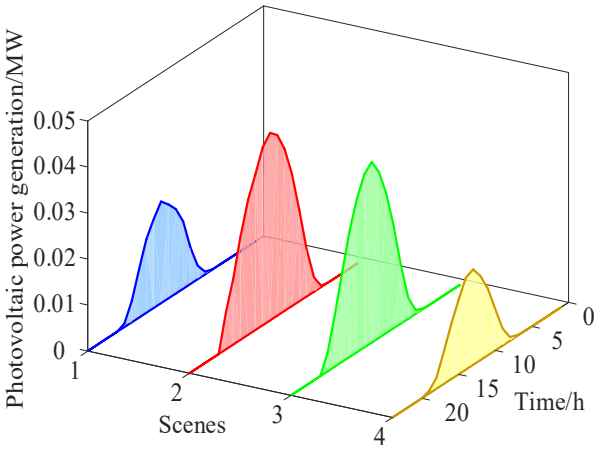


Figure 7. Photovoltaic power in typical scenarios.

2. Bi-Level Planning Results

For different scenarios, the results of energy router location and capacity configuration and the optimized operation of the active distribution network are presented in Tables 2 and 3.

Table 2. The results of energy router location and capacity under four schemes.

Scheme	Energy Router Number	Installation Site	Capacity/MVA
Scheme 1	1	8-node	3
	2	9-node	3.6
Scheme 2	1	13-node	4.2
	2	31-node	3
Scheme 3	1	13-node	4
	2	20-node	3
Scheme 4	1	14-node	4.2
	2	30-node	3.4

Table 3. The target solution results under the four schemes.

Scheme	Comprehensive Cost/Yuan	Investment Cost/Yuan	Operation and Maintenance Cost/Yuan	Response/Yuan	Network Loss/kW	Voltage Excursion/pu	Power Surge/kW
1	73,999.80	7868.8	66,131	0	1788.6	1.9305	3477.7
2	76,537.56	8584.1	64,042	3911.46	1778.2	1.5402	3315.6
3	74,935.70	8345.7	66,590	0	1775.4	1.2545	3108.4
4	77,609.82	9061.0	64,569	3979.82	1769.6	0.9733	2937.2

From Tables 2 and 3, it can be seen that when flexible load demand response is considered, the energy storage capacity configuration is larger, indicating that the energy router needs to have sufficient capacity to handle peak demands during load regulation and ensure stable power supply. Furthermore, compared to the single-scenario optimization, the energy storage capacities of Energy Router 1 and Energy Router 2 both increase under the multi-scenario optimization, suggesting that single-scenario optimization cannot meet the diverse load demands. Therefore, in a multi-scenario setting, the energy storage capacity needs to be adjusted to achieve more effective peak shaving and valley filling.

From Table 3, it is evident that the investment cost of Scenario 1 is lower than that of Scenario 2 and Scenario 3, while Scenario 3 has lower investment costs compared to Scenario 4. This indicates that with the introduction of demand response and multi-scenario optimization, the energy router's capacity configuration increases, leading to higher investment costs. In terms of operational and maintenance (O&M) costs, Scenario 1 has higher costs than Scenario 2, and Scenario 3 has higher costs than Scenario 4, indicating that the introduction of demand response effectively reduces O&M costs by appropriately adjusting part of the load to avoid peak hours. Regarding security indicators, multi-scenario optimization significantly reduces voltage deviations and network losses, and effectively smooths the load curve through peak shaving and valley filling. This demonstrates that multi-scenario optimization improves the overall system performance. Despite the higher investment costs due to demand response implementation, Scenarios 2 and 4 outperform Scenarios 1 and 3 in terms of voltage deviation improvement and peak shaving and valley filling.

In summary, Scenario 4, benefiting from both demand response and multi-scenario optimization, not only enhances the capacity configuration ability of the energy router but also significantly reduces system operation costs and improves operational efficiency. There-

fore, the combination of demand response and multi-scenario optimization significantly optimizes the energy router's location and capacity decision-making, comprehensively improving the overall performance of the power system.

3. Comparison of Peak Shaving and Valley Filling Effects and Voltage Deviation

To visually compare the optimized operation of the energy router in the active distribution network under different scenarios, a peak shaving and valley filling evaluation index was constructed, as shown in Equation (21):

$$\begin{cases} Y_1 = P_{\max} - P_{\min} \\ Y_2 = \frac{P_{\min}}{P_{\max}} \\ Y_3 = \frac{Y_1}{P_{\max}} \times 100\% \\ Y_4 = \frac{Y_1' - Y_1}{Y_1'} \times 100\% \end{cases} \tag{21}$$

In the formula, Y_1 is the absolute peak-valley difference; Y_2 is the peak-valley coefficient; Y_3 is the load peak-valley difference rate; Y_4 is the optimization rate of peak clipping and valley filling; Y_1' is the original absolute peak-valley difference. The peak shaving and valley filling effects for the four scenarios are shown in Table 4.

Table 4. Comparison of peak clipping and valley filling indexes under four schemes.

Scenario	Original Load Absolute Peak–Valley Difference/kW	Original Load Peak–Valley Difference Rate/%	Optimized Absolute Peak–Valley Difference/kW	Optimized Peak–Valley Factor	Optimized Peak–Valley Difference Rate/%	Optimization Rate/%
1	3954.7	44.64	3477.7	0.60	39.08	12.06
2	3954.7	44.64	3315.6	0.62	37.60	16.16
3	3423.3	41.43	3108.4	0.62	37.87	9.19
4	3423.3	41.43	2937.2	0.64	35.43	14.35

From Table 4, it can be seen that considering flexible load demand response improves the peak shaving and valley filling effects of the active distribution network. Specifically, Scenario 4 outperforms Scenario 3, and Scenario 2 is better than Scenario 1. In particular, the peak shaving and valley filling optimization rate in Scenario 4 is 14.3537%, significantly higher than Scenario 3's 9.1987%. This indicates that with flexible load demand response, the energy router can respond more flexibly to power fluctuations, balancing the variability of renewable energy, thus improving the grid's stability and economic efficiency.

Additionally, when comparing Scenario 1 and Scenario 3, although single-scenario optimization is superior in peak shaving and valley filling, multi-scenario optimization makes the energy router's capacity configuration more adaptable to meet different operational demands under varying load conditions.

Figures 8 and 9 illustrate the load curves and voltage deviation behavior before and after multi-scenario optimization with demand response. After multi-scenario optimization and the introduction of demand response, the load curve is significantly smoother, and the peak shaving and valley filling effect is enhanced. In the original case, the load curve exhibits significant fluctuations, especially during high-load periods, leading to increased pressure on power supply. After introducing multi-scenario demand response, the energy router dynamically adjusts the output of the energy storage unit according to load variations across different scenarios, effectively reducing the peaks and filling the valleys, achieving more efficient load regulation.

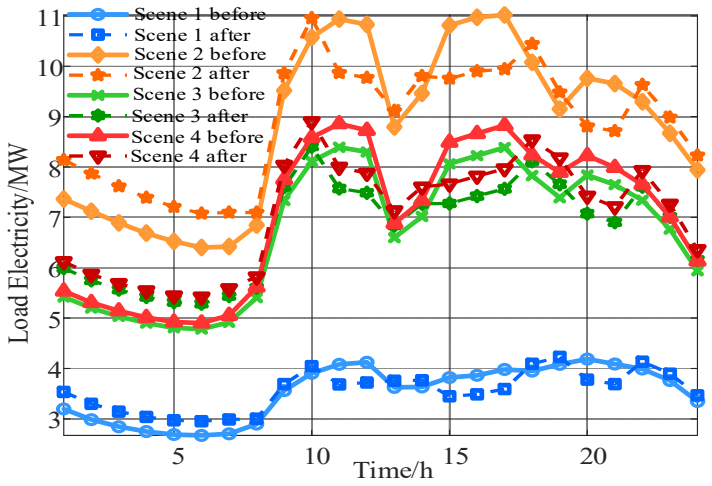


Figure 8. Load curve considering demand response.

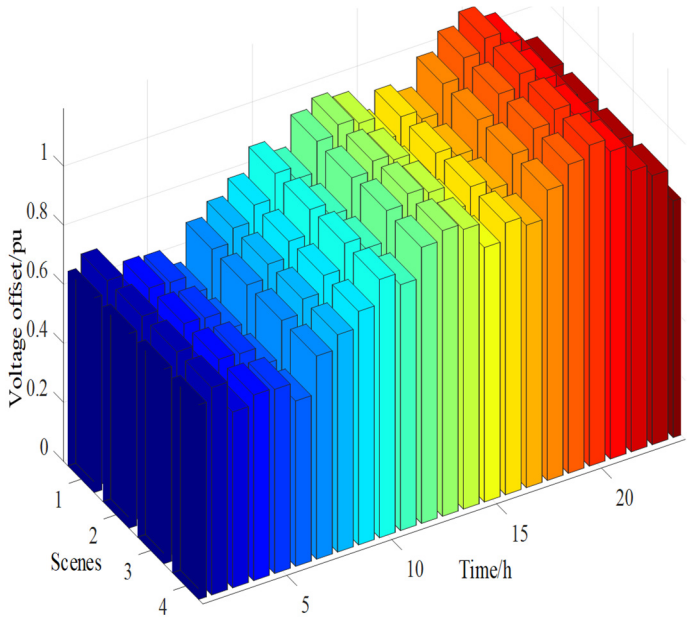


Figure 9. Considering the voltage offset under demand response.

Figure 9 shows the total voltage deviation at each time point in the distribution network after multi-scenario optimization. Under multi-scenario optimization, the energy router coordinates the dispatch of energy storage and renewable energy, maintaining a small and stable voltage deviation from 1 to 12 h, ensuring voltage stability. Although voltage deviation increases between 13 and 24 h due to higher load demands and renewable energy fluctuations, the collaboration between multi-scenario optimization and demand response significantly reduces voltage fluctuations. The energy router can adjust the energy storage and renewable energy outputs in real time to prevent excessive voltage deviation, ensuring stable grid operation during high-load periods.

5.4. Sensitivity Analysis of Flexible Load Ratio

To further assess the impact of flexible load participation on the energy router configuration strategy and system operating performance, a sensitivity analysis is conducted on the participation ratio of flexible loads. Building upon Scenario 4 as a baseline, the proportions of shiftable load and curtailable load within the total load are varied to examine their effects on key indicators such as siting and sizing schemes, system comprehensive cost, voltage deviation, and power fluctuation.

In the default setting, the flexible load ratio is defined as 30% for shiftable load and 15% for curtailable load. Based on this, the following four comparative scenarios are established:

Scenario 1: Shiftable load accounts for 10% of the flexible load, and curtailable load accounts for 5%.

Scenario 2: Shiftable load accounts for 20% of the flexible load, and curtailable load accounts for 10%.

Scenario 3: Shiftable load accounts for 30% of the flexible load, and curtailable load accounts for 15%.

Scenario 4: Shiftable load accounts for 40% of the flexible load, and curtailable load accounts for 20%.

A two-layer optimization for ER siting and sizing is performed under different flexible load ratios, and the resulting configuration is shown in Table 5. As the flexible load participation ratio increases, the ER siting and capacity configuration exhibit some degree of adjustment. With the support of a high-ratio response capability, the system's dependence on energy storage resources decreases, causing the ER configuration capacity to show a decreasing trend. This change indicates that enhanced load regulation capabilities can, to some extent, replace the physical support of energy storage facilities, thereby effectively reducing system investment requirements and configuration costs. Simultaneously, the improvement in the flexible load level also affects the selection of the optimal access node for the ER, reflecting its feedback effect on the system's operating state and further validating the necessity of collaborative optimization of multi-source loads in practical applications.

Table 5. The results of the ER siting and capacity allocation for different flex load participation ratios.

Scheme	Energy Router Number	Installation Site	Capacity/MVA
Scheme 1	1	14-node	4.5
	2	9-node	4.2
Scheme 2	1	27-node	4.2
	2	9-node	3.6
Scheme 3	1	14-node	4.2
	2	30-node	3.4
Scheme 4	1	9-node	3.8
	2	20-node	2.8

From the perspective of operating performance, as shown in Table 6, the improvement of the flexible load ratio significantly improves the overall operating performance of the system. Specifically, the comprehensive cost gradually decreases from Scenario 1 to Scenario 4, with a cumulative decrease of approximately 4.4%. Although the response incentive cost increases, the investment and operation and maintenance costs decrease simultaneously, reflecting the cost advantage of load-side regulation in alleviating system operating pressure. Furthermore, the magnitude of power fluctuation decreases significantly, indicating that the system load curve tends to be smoother, and peak shaving and valley filling capabilities are significantly enhanced. The voltage deviation and network loss indicators also improve accordingly, further verifying the role of flexible loads in improving power quality and system stability.

In summary, as the flexible load participation ratio increases, the flexibility, economic efficiency, and security of system operation are all enhanced, fully illustrating the positive significance of introducing demand response mechanisms in active distribution networks for the optimized configuration of energy routers and system operation scheduling.

Table 6. The results of multi-objective solving with different flexible load participation ratios.

Scheme	Comprehensive Cost/Yuan	Investment Cost/Yuan	Operation and Maintenance Cost/Yuan	Response/Yuan	Network Loss/kW	Voltage Excursion/pu	Power Surge/kW
1	79,051.33	10,372.5	66,314	2364.83	1773.3	1.0572	3556.1
2	76,564.49	9299.4	64,268	2997.09	1772.5	1.0437	3347.8
3	77,609.82	9061.0	64,569	3979.82	1769.6	0.9733	2937.2
4	75,535.21	7868.8	62,673	4993.41	1768.2	0.9481	2249.6

5.5. Comparison of Different Solution Algorithms

To evaluate the optimization performance of the improved bi-level particle swarm optimization (PSO) algorithm, this paper compares it with the traditional bi-level PSO and simulated annealing-particle swarm hybrid optimization algorithm. The population size for both upper and lower layers is set to 50, with 30 iterations for the lower layer. For each iteration of the upper layer, the lower layer performs 30 iterations. All algorithms were independently executed 30 times on the MATLAB 2023a platform, and the results are shown in Table 7, with iteration curves depicted in Figure 10.

Table 7. Comparison of results of different solving algorithms.

Algorithm	Comprehensive Cost/Yuan	Number of Upper Convergence Iterations (Including Lower 30)	Convergence Time/s
Improved bi-level PSO	82,318	10	6906
Traditional bi-level PSO	90,542	18	11,933
Simulated annealing—particle swarm	89,579	15	8150

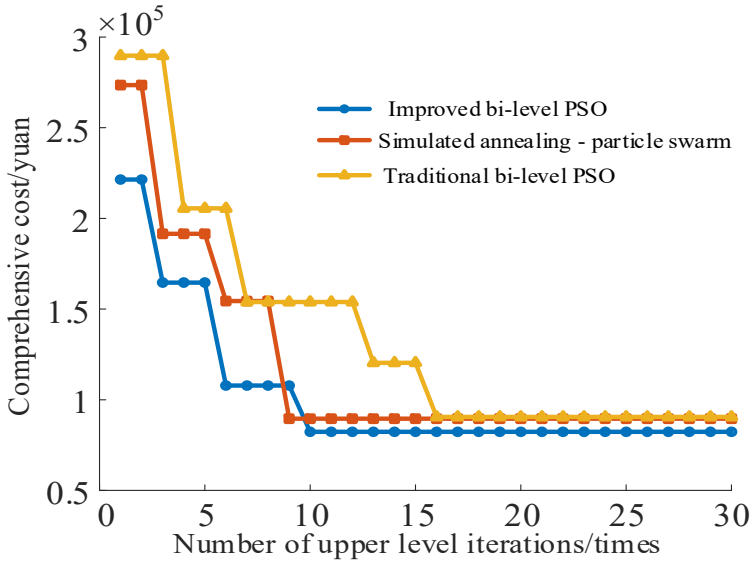


Figure 10. The upper iterative curves of different algorithms.

The results indicate that the improved bi-level PSO algorithm reduces the number of iterations and convergence time by 44.4% and 42.1%, respectively, compared to the traditional bi-level PSO. In comparison with the simulated annealing-particle swarm hybrid optimization algorithm, the reductions are 33.3% and 15.3%, respectively. Furthermore, the improved algorithm achieves better performance in terms of the optimal objective function value, demonstrating that the multi-strategy fusion mechanism significantly enhances the optimization efficiency and solution accuracy of the bi-level PSO algorithm.

6. Conclusions

To address issues such as insufficient wind and solar energy accommodation, elevated network losses, and significant load fluctuations in active distribution networks, this paper proposes an optimized energy router (ER) configuration method incorporating flexible load demand response. The following conclusions are drawn:

(1) Multi-Scenario Clustering and Demand Response Optimize ER Capacity: The combination of multi-scenario clustering and demand response optimizes the capacity configuration strategy of the energy router, significantly enhancing the system's adaptability to various load operating states. Compared to traditional single-scenario optimization methods, energy storage unit configuration under multi-scenario optimization is more reasonable, enabling better handling of complex operating conditions. While the increased equipment capacity leads to a certain increase in investment costs, system operation and maintenance costs are effectively reduced, and voltage deviation and load balance problems are significantly improved, resulting in a marked improvement in overall operating efficiency.

(2) ER Integration Enhances Peak Shaving and Renewable Energy Consumption: Under multi-scenario optimization, the integration of the energy router into the active distribution network effectively enhances peak shaving and valley filling capabilities, achieving an optimization rate of 9.19%, which further increases to 14.35% when combined with demand response. Concurrently, the consumption capacity of renewable energy is enhanced, system network losses are significantly reduced, and power quality is effectively improved, thereby increasing the operational safety and economic efficiency of the distribution system. This method is suitable for various practical scenarios, including urban distribution networks, industrial park microgrids, and areas with high renewable energy penetration, providing a feasible path for achieving low-carbon and intelligent control of active distribution networks.

(3) Improved Bi-Level PSO Algorithm: The improved bi-level particle swarm optimization algorithm integrates multiple strategies, significantly enhancing search capabilities and accelerating the convergence process. Compared to simulated annealing-particle swarm hybrid optimization and traditional bi-level particle swarm algorithms, this algorithm reduces the average number of iterations by 44.4% and 33.3%, respectively, and shortens the convergence time by 42.1% and 15.3%, validating its advantages in terms of search efficiency and convergence performance.

(4) Sensitivity Analysis Reveals Impact of Flexible Load Participation: Sensitivity analysis of different flexible load ratios reveals that as the response level increases, both the location and capacity configuration of the ER undergo changes, and the system's dependence on energy storage units decreases, leading to a more compact and reasonable configuration. Simultaneously, system operating performance continuously improves, comprehensive costs are reduced by approximately 4.4%, power fluctuations are significantly reduced, and peak shaving and valley filling effects are markedly enhanced. Flexible loads enhance regulation and enable balanced resource allocation and performance optimization, supporting collaborative demand response in active distribution networks.

This study does not delve into the impact of demand response on user satisfaction and willingness to participate, particularly its effect on the optimization of the bi-level planning model. Future research could further integrate user behavior models to analyze the influence of demand response incentive mechanisms on the optimization results, enhancing the practical feasibility and user acceptance of energy router planning and scheduling.

Author Contributions: Conceptualization, J.J. (Junqing Jia); methodology, Z.W. and J.L.; software, C.S.; validation, Z.W.; formal analysis, T.W.; investigation, J.Z.; project administration, J.J. (Jiaoxin Jia); resources, J.J. (Junqing Jia); data curation, T.W.; writing—original draft preparation, J.J. (Junqing Jia) and T.W.; writing—review and editing, W.C. and J.J. (Jiaoxin Jia); visualization, J.L.; supervision, W.C.; funding acquisition, J.J. (Jiaoxin Jia). All authors have read and agreed to the published version of the manuscript.

Funding: The authors gratefully acknowledge the financial support of Inner Mongolia (Electric Power) Group Limited Liability Company (2024-4-47).

Data Availability Statement: The data presented in this study are available on request from the corresponding author. The data are not publicly available due to institutional restrictions.

Conflicts of Interest: Junqing Jia, Tianyu Wu and Jia Zhou were employed by Inner Mongolia Electric Power (Group) Co., Ltd. The remaining authors declare that the research was conducted in the absence of any commercial or financial relationships that could be construed as a potential conflict of interest. The funders had no role in the design of the study; in the collection, analyses, or interpretation of data; in the writing of the manuscript, or in the decision to publish the results.

References

1. Choobdari, M.; Moghaddam, M.S.; Davarzani, R.; Azarfar, A.; Hoseinpour, H. Robust distribution networks reconfiguration considering the improvement of network resilience considering renewable energy resources. *Sci. Rep.* **2024**, *14*, 23041. [CrossRef] [PubMed]
2. Kyriakou, D.G.; Kanellos, F.D. Sustainable operation of active distribution networks. *Appl. Sci.* **2023**, *13*, 3115. [CrossRef]
3. Tang, M.; Lau, V.K.N. Decentralized event-triggered scheduling and control for multiagent linear systems over wireless interference channels. *IEEE Trans. Control Netw. Syst.* **2022**, *9*, 1348–1361. [CrossRef]
4. Tang, M.; Cai, S.; Lau, V.K.N. Online system identification and control for linear systems with multiagent controllers over wireless interference channels. *IEEE Trans. Autom. Control* **2022**, *68*, 6020–6035. [CrossRef]
5. Bakry, O.M.; Alhabeeb, A.; Ahmed, M.; Alkhalaf, S.; Senjyu, T.; Mandal, P.; Dardeer, M. Improvement of distribution networks performance using renewable energy sources based hybrid optimization techniques. *Ain Shams Eng. J.* **2022**, *13*, 101786. [CrossRef]
6. Cavalheiro, E.M.B.; Vergilio, A.H.B.; Lyra, C. Optimal configuration of power distribution networks with variable renewable energy resources. *Comput. Oper. Res.* **2018**, *96*, 272–280. [CrossRef]
7. Azmi, K.H.M.; Radzi, N.A.M.; Azhar, N.A.; Samidi, F.S.; Zulkifli, I.T.; Zainal, A.M. Active Electric Distribution Network: Applications, Challenges, and Opportunities. *IEEE Access* **2022**, *10*, 134655–134689. [CrossRef]
8. Zhu, H.; Chen, S.; Yu, Y.; Zhao, H.; Zhang, J.; Yi, R. Research Status and Prospects of Key Technologies for Electric Energy Router. In Proceedings of the 2023 6th International Conference on Electronics Technology (ICET), Chengdu, China, 12–15 May 2023; pp. 830–835.
9. Liu, Y.; Fang, Y.; Li, J. Interconnecting microgrids via the energy router with smart energy management. *Energies* **2017**, *10*, 1297. [CrossRef]
10. Zhou, J.; Wang, J. Research review on multi-port energy routers adapted to renewable energy access. *Electronics* **2024**, *13*, 1493. [CrossRef]
11. Chen, M.; Xia, M.; Chen, Q. Research on distributed source-load interaction strategy considering energy router-based active distribution network. *IEEE Access* **2019**, *7*, 150505–150516. [CrossRef]
12. Miao, J.; Zhang, N.; Kang, C. Analysis on the influence of energy router on the optimal operation of distribution network. *Proc. CSEE* **2017**, *37*, 2832–2839.
13. Geng, Q.; Hu, Y.; He, J.Z.; Zhou, Y.X.; Zhao, W. Optimal power flow for hybrid AC/DC grid with power electronic transformer. *Power Syst. Technol.* **2019**, *43*, 3288–3296.
14. Chen, M.; Xia, M.; Chen, Q. Two-stage Planning Method for Energy Router Considering Its Optimal Operation in Distribution Networks. *CSEE J. Power Energy Syst.* **2022**, *10*, 605–616.
15. Geng, Q.; Hu, Y.; He, J.; Zhou, Y.; Zhao, W.; Xu, X.; Wei, W. Optimal operation of AC–DC distribution network with multi park integrated energy subnetworks considering flexibility. *IET Renew. Power Gener.* **2020**, *14*, 1004–1019. [CrossRef]
16. Peng, Q.; Qu, L.; Yuan, Z.; Wang, X.; Chen, Y.; Tian, B. Optimal scheduling strategy of AC/DC hybrid distribution network based on power electronic transformer. *Energies* **2021**, *14*, 3219. [CrossRef]
17. Li, Z.; Ye, P.; He, J.; Yin, Y. Research on Energy Router-Based Coordination of Integrated Energy System and Distribution Network. In Proceedings of the 2023 IEEE 5th International Conference on Power, Intelligent Computing and Systems (ICPICS), Shenyang, China, 14–16 July 2023; pp. 384–387.

18. Guo, X.; Gan, L.; Liu, Y.; Hu, W. Coordinated dispatching of flexible AC/DC distribution areas considering uncertainty of source and load. *Electr. Power Syst. Res.* **2023**, *225*, 109805. [CrossRef]
19. Dong, L.; Zhang, T.; Pu, T.; Chen, N.; Sun, Y. A decentralized optimal operation of AC/DC hybrid microgrids equipped with power electronic transformer. *IEEE Access* **2019**, *7*, 157946–157959. [CrossRef]
20. Huang, L.; Li, Y.; Cui, Q.; Xie, N.; Zeng, J.; Shu, J. Research on optimal configuration of AC/DC hybrid system integrated with multiport solid-state transforms and renewable energy based on a coordinate strategy. *Int. J. Electr. Power Energy Syst.* **2020**, *119*, 105880. [CrossRef]
21. Zhao, Z.; Feng, G.; Yuan, L.; Zhang, C. The development and key technologies of electric energy router. *Proc. CSEE* **2017**, *37*, 3823–3834.
22. Georgilakis, P.S.; Hatziargyriou, N.D. A review of power distribution planning in the modern power systems era: Models, methods and future research. *Electr. Power Syst. Res.* **2015**, *121*, 89–100. [CrossRef]
23. Guo, Z.; Zhang, R.; Wang, L.; Zeng, S.; Li, Y. Optimal operation of regional integrated energy system considering demand response. *Appl. Therm. Eng.* **2021**, *191*, 116860. [CrossRef]
24. Hou, L.; Tong, X.; Chen, H.; Fan, L.; Liu, T.; Liu, W.; Liu, T. Optimized scheduling of smart community energy systems considering demand response and shared energy storage. *Energy* **2024**, *295*, 131066. [CrossRef]
25. Chreim, B.; Esseghir, M.; Merghem-Boulahia, L. LOSISH—LOad Scheduling In Smart Homes based on demand response: Application to smart grids. *Appl. Energy* **2022**, *323*, 119606. [CrossRef]
26. Sinaga, K.P.; Yang, M.S. Unsupervised K-means clustering algorithm. *IEEE Access* **2020**, *8*, 80716–80727. [CrossRef]
27. Chamandoust, H.; Bahramara, S.; Derakhshan, G. Day-ahead scheduling problem of smart micro-grid with high penetration of wind energy and demand side management strategies. *Sustain. Energy Technol. Assess.* **2020**, *40*, 100747. [CrossRef]
28. Ali, S.; Ullah, K.; Hafeez, G.; Khan, I.; Albogamy, F.R.; Haider, S.I. Solving day-ahead scheduling problem with multi-objective energy optimization for demand side management in smart grid. *Eng. Sci. Technol. Int. J.* **2022**, *36*, 101135. [CrossRef]
29. Xu, X.-F.; Wang, K.; Ma, W.-H.; Wu, C.-L.; Huang, X.-R.; Ma, Z.-X.; Li, Z.-H. Multi-objective particle swarm optimization algorithm based on multi-strategy improvement for hybrid energy storage optimization configuration. *Renew. Energy* **2024**, *223*, 120086. [CrossRef]
30. Ma, M.; Wu, J.; Shi, Y.; Yue, L.; Yang, C.; Chen, X. Chaotic random opposition-based learning and Cauchy mutation improved moth-flame optimization algorithm for intelligent route planning of multiple UAVs. *IEEE Access* **2022**, *10*, 49385–49397. [CrossRef]

Disclaimer/Publisher's Note: The statements, opinions and data contained in all publications are solely those of the individual author(s) and contributor(s) and not of MDPI and/or the editor(s). MDPI and/or the editor(s) disclaim responsibility for any injury to people or property resulting from any ideas, methods, instructions or products referred to in the content.